Analysis of Brushed DC Machinery Faults With Coupled Finite Element Method and Equivalent Circuit Model

Todd D. Batzel, Nicholas C. Becker, and Mihai Comanescu,
Pennsylvania State University, Altoona College
tdb120@psu.edu, ncb5040@psu.edu, muc23@psu.edu

Abstract

Although brush type DC machinery has lost market share over the years to its brushless counterparts, it still maintains a significant presence in the automotive, aerospace, power tool, and home appliance industries. Especially in automotive and aerospace power system applications, early detection of brush type DC machine faults will help to avoid problematic system failures, decrease maintenance costs, and increase system reliability. This paper focuses on a modeling approach that is used to investigate the effects of various fault mechanisms of the brushed DC machine at an early stage in their progression. Results from the proposed model are then used to show the effects of a variety of DC machine failure modes and identify observable parameters to assist in early fault detection. The simulation results are then confirmed through laboratory experiments performed on a DC generator.

Introduction

The brushed DC machine is still widely used in automotive and aerospace systems as an actuator, starter, generator or starter/generator. The detection of impending failures associated with brush type DC machines can be used to draw attention to the need for maintenance and therefore reduce the possibility of a catastrophic system breakdown. In this paper, a modeling approach is developed to investigate the effects of various fault mechanisms of the machine and identify measurable parameters that can be used as indicators of a developing fault.

Although research in this area is sparse, investigation of DC machine failure modes have been reported in the literature. In [1] and [2], a mathematical model is used to investigate the effects of short- and open-circuit armature coils. Position-dependent machine inductances used in this model were pre-determined using finite element analysis, and brushes are approximated by a variable resistance. Experimental results suggest that field current harmonics can be used to indicate armature coil short circuits. However, armature open circuits were virtually undetectable. The approach was modified [3] to include saturation effects using a winding function approach.

In [4], a lumped parameter mathematical model, including mechanical parameters inertia and friction, is used to detect brushed permanent magnet DC machine faults. This proposed technique uses the starting current transient as an indicator of open- and short-circuited armature coils and brush wear. Application of this method is limited to systems where mechanical parameters are well known.

The amount of sparking at the brushes in a DC machine is an accepted measure of commutation quality, and therefore may be used as an indicator of excessive brush wear. The work in [5] and [6] both present methods for monitoring the sparking index in the brush DC motor.

In this paper, a lumped parameter circuit model is used where each individual armature coil is placed based on the present commutation state. The resulting differential equation model is coupled with a time-stepping finite element analysis to obtain a solution for armature and field voltages and currents. The model, which is readily modifiable to analyze machine faults, is then used to evaluate performance at the onset of faults such as armature open and short circuits, field winding short circuits, commutator segment failures, and brush degradation. The information from these simulations is then used to identify observable parameters that can detect and classify the onset of brushed DC machine failures.

DC Machine Mathematical Equations

Fig. 1 shows the armature coil and commutator segment connections of a two-pole brush DC generator with 12 coils and commutator segments. Coil position in the armature slots is shown in Fig. 2, where a double-layer lap winding is used and each coil consists of 15 series wound conductors. A single brush pair is employed. The voltage across each of j coils in Fig. 1 is

$$v_j = e_j + i_j R_j = \frac{d\lambda_j}{dt} + i_j R_j \ ,$$

(1)

where v, e, i, and R represent the terminal voltage, induced emf, current, and resistance, respectively, of the coil. For a 12-coil machine with a wound field, the flux linkages can be represented in matrix form by (2) where θ is the angle between the magnetic axis of the field winding and rotating coil 1.
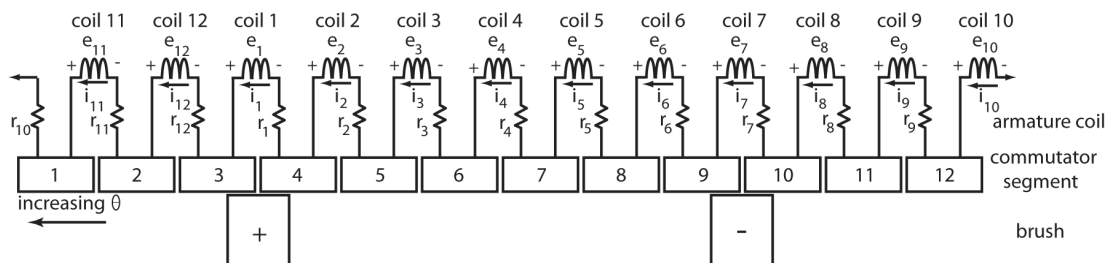

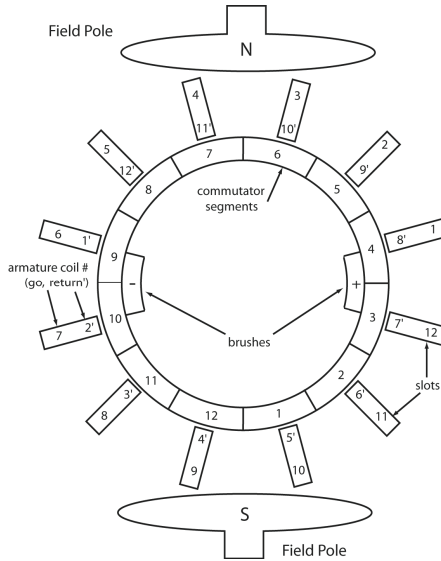Figure 1: Coil and commutator segment connections for DC generator

Figure 2: Coil placement in armature

$$
\begin{bmatrix} \lambda_1 \\ \lambda_2 \\ M \\ \lambda_{12} \\ \lambda_f \end{bmatrix} = \begin{bmatrix} L_{1,1} & L_{1,2} & L & L_{1,12} & L_{1,f}\cos(\theta) \\ L_{2,1} & L_{2,2} & L & L_{2.12} & L_{2,f}\cos(\theta-30^{0}) \\ M & M & O & M & M \\ L_{12,1} & L_{12,2} & L & L_{12,12} & L_{12,f}\cos(\theta+30^{0}) \\ L_{f,1}\cos(\theta) & L_{f,2}\cos(\theta-30^{0}) & L & L_{f,12}\cos(\theta+30^{0}) & L_{f,f} \end{bmatrix} \begin{bmatrix} i_1 \\ i_2 \\ M \\ i_{12} \\ i_f \end{bmatrix} \quad (2)
$$

For simplicity, the self and mutual inductances between all armature coils are considered to be constant, while all mutual inductances between the field winding and armature coils are a function of the rotor angle. Vector notation (2) can be simplified to:

$$
\lambda = \mathbf{L}(\theta)\mathbf{i}. \tag{3}
$$

The induced emf vector *e* in (1) is determined by:

$$
\mathbf{e} = \frac{d}{dt}\lambda = \omega \mathbf{L'i} + \mathbf{L}\frac{d}{dt}\mathbf{i} = e_\omega + e_L. \tag{4}
$$

The first term on the right side of (4) represents voltage induced by armature rotation, while the second is due to inductive (self and mutual) coupling between coils.

Simplified DC Machine Circuit Model

A simplified model for the DC machine is now presented. The analytical circuit model for a sample DC Generator (with 12 armature coils) is shown in Fig. 3. In this model, an index,
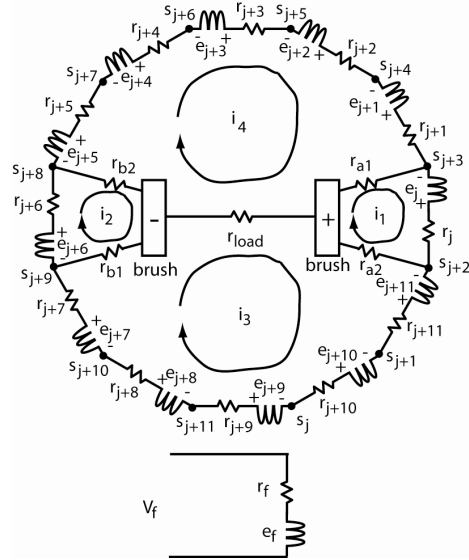
Figure 3: Circuit Model for Brush DC

j=1 through 12, is used to identify each coil and commutator segment s. The modulo 12 index is assigned based on rotor position θ according to Table 1. The resistances r_{a1}, r_{a2}, r_{b1}, and r_{b2} represent the brush-to-commutator contact resistance, which is determined based on rotor position, contact surface area, and current density [7]. The contact conductance for a healthy brush at nominal current density is shown in Fig. 4, where it is assumed that the brush never contacts three segments simultaneously. The term g_{max} is used to represent the maximum brush-to-commutator conductance, which occurs when the brush has maximum contact area with the commutator. The use of a lookup table to identify conductances makes it relatively simple to model certain aspects of brush and commutator wear.

The model of Fig. 3 can be further simplified by combining series-connected coils, where the coils connected in series depend on the present brush position. The resulting simplified model is shown in Fig. 5, where $e_{\omega n}$, L_n, and r_n (n=1 to 4) represent the induced motional emf, the inductance terms, and resistance of the equivalent coils, respectively, at any rotor position. Applying mesh analysis to the circuit of Fig. 5 and including the mutual inductance
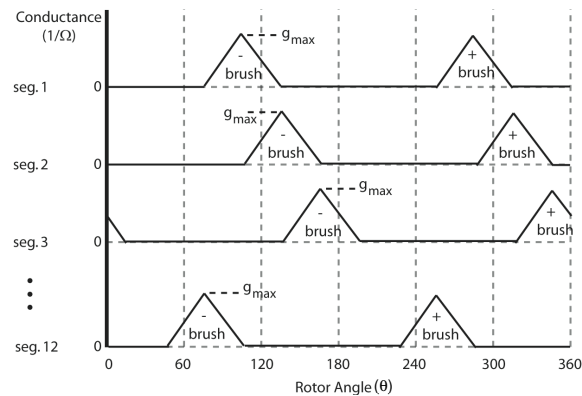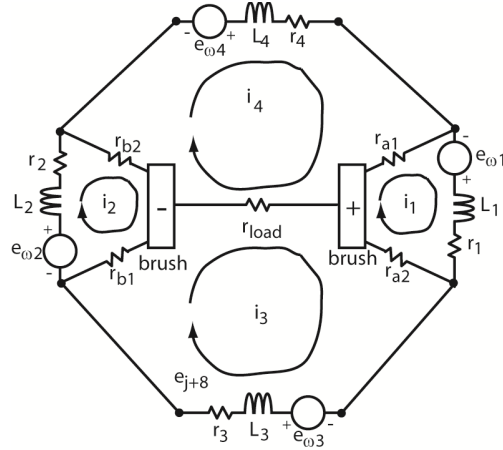

Figure 4: Brush to segment resistances

Figure 5: Circuit Model for Brush DC

terms that are not obvious from the circuit diagram yields (5), where $e_{\omega 1}$ and $e_{\omega 2}$ represent the induced voltages due to motion only in the branches undergoing commutation, while $e_{\omega 3}$ and $e_{\omega 4}$ are the sum of voltages induced due to motion only in the series connected armature branches not under commutation. The subscripts 1 through 4 have similar meaning when used with the branch currents, resistances, and inductances.

$$
\begin{vmatrix} e_{\omega 1} \\ e_{\omega 2} \\ e_{\omega 3} \\ e_{\omega 4} \\ V_f - e_f \end{vmatrix} = \begin{vmatrix} (r_1 + r_{a1} + r_{a2}) & 0 & -r_{a2} & -r_{a1} & 0 \\ 0 & (r_2 + r_{b1} + r_{b2}) & -r_{b1} & -r_{b2} & 0 \\ -r_{a2} & -r_{b1} & (r_3 + r_{b1} + r_{a2} + r_{load}) & -r_{load} & 0 \\ -r_{a1} & -r_{b2} & -r_{load} & (r_4 + r_{a1} + r_{b2} + r_{load}) & 0 \\ 0 & 0 & 0 & 0 & R_f \end{vmatrix} \begin{vmatrix} i_1 \\ i_2 \\ i_3 \\ i_4 \\ i_f \end{vmatrix}
$$

$$
+ \begin{bmatrix} L_{11} & -L_{12} & 0 & 0 & -L_{1f} \\ -L_{21} & L_{22} & 0 & 0 & L_{2f} \\ 0 & 0 & L_{33} & -L_{34} & 0 \\ 0 & 0 & -L_{43} & L_{44} & 0 \\ -L_{f1} & L_{f2} & 0 & 0 & L_{ff} \end{bmatrix} \frac{d}{dt} \begin{bmatrix} i_1 \\ i_2 \\ i_3 \\ i_4 \\ i_f \end{bmatrix}
$$

(5)

In vector form, (5) is:

$$\mathbf{e}_\omega = \mathbf{r}\mathbf{i} + \mathbf{L}\frac{d}{dt}\mathbf{i} \tag{6}$$

Time-Stepping DC Machine Analysis

The DC machine is modeled using magnetostatic FEA tools [8] coupled with the differential circuit equation given by (6). The magnetostatic FEA is capable of determining the instantaneous self and mutual inductance terms and the motional emf (e_ω) terms of (6). To obtain the machine state at each time step, the FEA program first uses the present current vector to compute e_ω, **L**, and **r** based on the brush position and angular velocity. With these
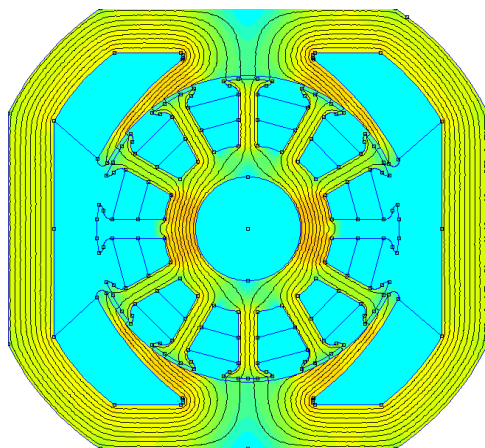
Figure 6: Magnetic FEA flux vector results at a single time step

FEA results, the differential equation identified by eq. (6) is used to update the current
vector. The current determined at each time step becomes the initial condition for the
following time step. The magnetostatic FEA tools used in the analysis can be used to
determine the motional voltage, but voltages due to self and mutual inductances must be
incorporated into the differential equations linking the FEA result to the time-stepping
analysis. The inductance values at each step are determined by FEA [9].

As an example, the magnetic flux vector calculated by FEA at a single time step is shown in
Fig. 6. The magnetic flux and the machine state variables at that time step allows calculation
of all coil voltages. Once the induced (due to mechanical motion) coil voltages are
determined, the rotor position dictates the electrical circuit configuration (which is brush
position dependent). The resulting circuit configuration is then solved using standard circuit
analysis techniques.

In summary, the FEA calculation and associated circuit analysis performed at a progression
of time steps yields armature voltage, armature current, field voltage, field current, and even
quantities that would not be feasible to measure on a physical system—such as the current in
an individual coil. Using this approach, it is rather straightforward and relatively fast to
analyze a DC machine operating as motor or generator under various conditions—even for
conditions such as winding failures or brush/commutator defects.

Fault Simulations for DC Machine

Coupled FEA simulations were performed on a DC machine operating as a starter/generator
for normal (baseline) operation as well as a variety of winding and brush/commutator failure
modes. Scenarios evaluated include:
- field winding short circuit
- armature winding faults
- brush resistance increase (uneven wear)
- commutator bar short circuit
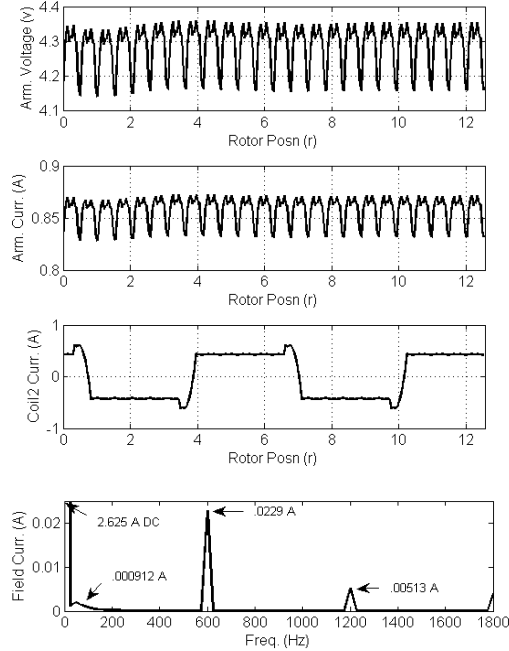- commutator bar open (bad segment)

Figure 7: Baseline simulation results

Each of these scenarios was evaluated at various operating speeds and load currents to determine observable quantities that are indicative of the respective failure mode. Baseline simulations were first performed to characterize the operation of a healthy DC machine. Although simulations were conducted for various operating conditions, for purposes of comparison all results will be shown with the DC machine acting as a generator at a speed of 3000 RPM, a load of 5 ohm, and a constant applied field voltage. For this rotational speed, the 2-pole machine with 12 commutator segments has a pole-passing frequency of 100 Hz and a commutation frequency of 600 Hz. Fig. 7 shows the armature voltage and current, the current in a single coil (which can't easily be measured physically), and the field current FFT. Note the presence of the commutation frequency in both the armature and field current.

Operation with a field winding short circuit was then simulated by altering the winding structure of the FEA machine description. Fig. 8 shows the results of a simulation with 12% of field windings short-circuited. When comparing the baseline result of Fig. 7 with the field winding short circuit, note that less armature voltage is produced relative to the field current magnitude with a shorted field winding. This results in the first identified observable called the *transfer impedance*, which is defined as the ratio of the induced armature voltage relative to the field current. The decrease in the transfer impedance when the field winding is short-circuited is readily explained. With fewer field turns available to produce magnetic flux at any reference speed, the induced voltage is reduced by Faraday's law. Since the induced armature voltage is also speed dependent, the transfer impedance is normalized relative to some reference speed ω_r so that the transfer impedance is calculated by

$$\frac{e_a}{i_f}\left(\frac{\omega}{\omega_r}\right),$$ (7)

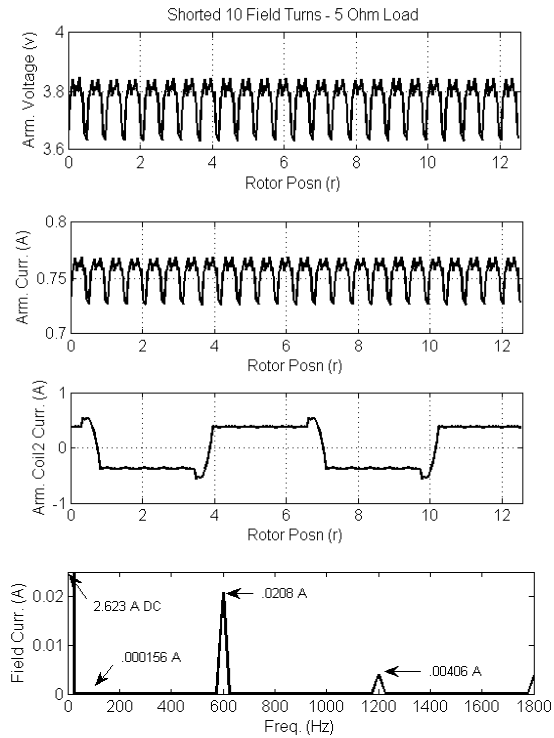where ω is the actual velocity.

Figure 8: Simulation of field winding short

Simulations of armature winding failures were then performed. Results for short-circuit (5.6% of armature turns) and open-circuit (single coil) armature are shown in Fig. 9 and 10,
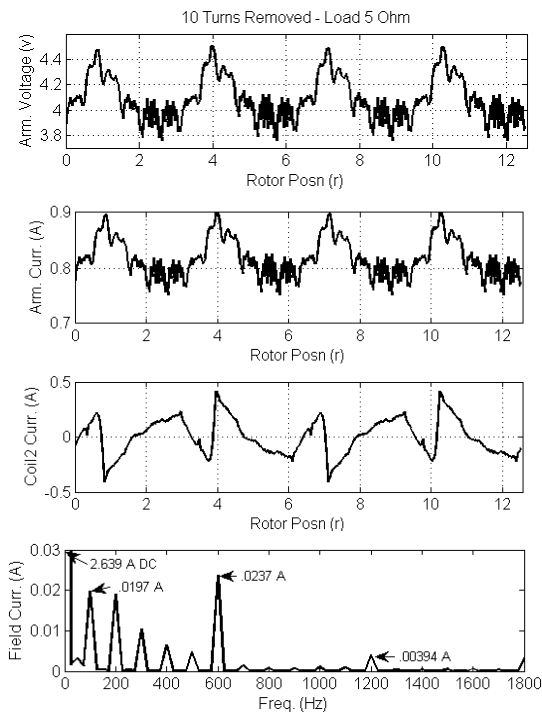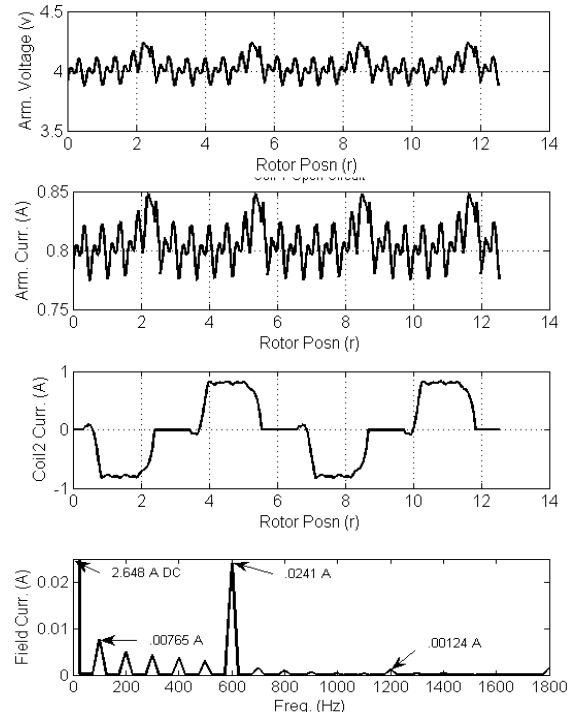

Figure 9: Simulation of armature short circuit

Figure 10: Simulation of arm. open circuit

respectively. In both cases, there is a marked increase in the field current at the pole-passing frequency as compared to baseline performance. This increase also concurs with the results shown in [2]. Thus, the pole-passing frequency component of the field current is an observable parameter that indicates a possible armature circuit problem. The pole-passing frequency component of the field current is defined as the number of poles of the starter/generator multiplied by the rotational speed in revolutions per second:

$$\text{pole-passing freq.} = \omega\,(\#\text{ poles}) . \tag{8}$$

This parameter is obtained by performing an FFT on the field current and then determining the amplitude of field current at the pole-passing frequency.

Commutator segment faults were then simulated. A commutator segment that does not make contact with the brush was simulated with results shown in Fig. 11. A significant pole-passing component (and harmonics) of field current is again developed as a result of this bad commutator segment. In addition, a field current component at the commutation frequency of 600 Hz appears. The commutation frequency, similar to the pole-passing frequency, uses the number of commutator segments on the machine:

$$\text{commutation freq.} = \omega\,(\#\text{ commutator bars}). \tag{9}$$

Physically, the field winding contains useful information about commutation because the armature coils undergoing commutation (i.e., the coils shorted by the brushes) are well coupled magnetically with the field winding.

Since a short circuit across adjacent commutator segments is similar to a short-circuited armature coil shown in Fig. 9, those results are not included here.
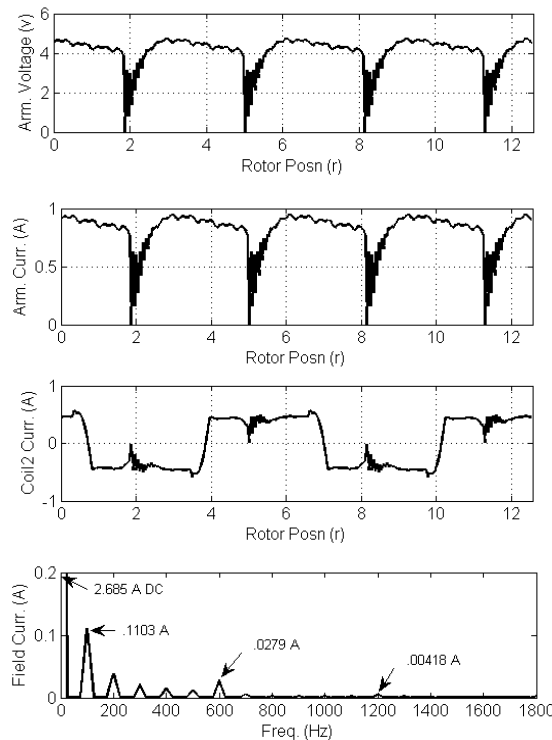

Figure 11: Open commutator segment simulation

Finally, simulations were performed to analyze the case where brush resistance is increased. This may occur for several reasons, such as decreased brush pressure or poor filming of the brush/commutator interface. The result of a 22% increase in brush contact resistance is shown in Fig. 12. Though there is little visible difference between the baseline results and Fig. 12, the transfer impedance is indeed reduced to 1.73 from its baseline value of 1.77 as brush resistance increases. Physically, this drop in transfer impedance occurs due to the increased drop in potential across the brushes. This effect is increasingly observable under higher load conditions.

A summary of the various faults and associated observables determined through the coupled FEA simulations is given in Table 2.

Table 2: DC machine fault observables

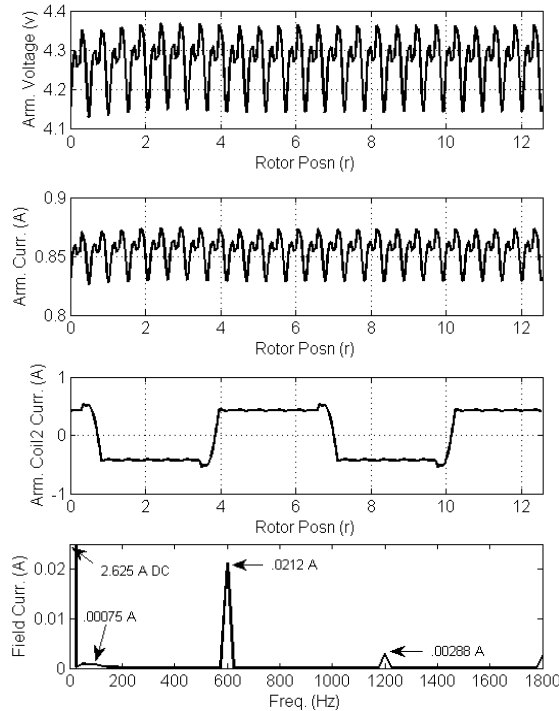| Fault Type	Transfer Imped. (e/i_f)	i_f at pole-passing	i_f at comm frq.
Field Short	decrease	no change	no change
Arm Short	decrease	increase	no change
Arm Open	decrease	increase	no change
Bad Comm Seg	decrease	major increase	small increase
Comm Seg Short	decrease	major increase	no change
Brush Wear	slight decrease	no change	no change

Figure 12: Increased brush resistance simulation

Seeded Fault Laboratory Experiments

As a follow-up to the FEA simulations, a series of laboratory experiments were performed on a DC machine to confirm the simulation results. For these tests, the faults used for simulations were, when feasible, seeded into the machine. For each case, a 4-pole DC machine with 72 commutator segments was operated at 1800 RPM and a load of 12.5 ohms. Thus, the pole-passing frequency is 120 Hz, and the commutation frequency is 2160 Hz. Except for the shorted armature coil test, the output voltage was regulated to 120v. The armature of the DC machine used in these experiments is shown in Fig. 13.

Baseline operation of the experimental DC machine is shown in Fig. 14. For baseline operation of this experimental DC machine, the transfer impedance was found to be 217.3.

Following the baseline test, a short circuit of approximately 10% of the field winding coils was established. The results, as shown in Fig. 15, demonstrate that to maintain the nominal output voltage of 120v, a much higher field current is required. This yields reduced transfer impedance as predicted by the FEA. Specifically, the transfer impedance in this case drops to 180 from its baseline of 217.3.

Shorted armature coil experimental results are shown in Fig. 16. For this test, a reduced field current is used to avoid permanent damage to the armature due to high short-circuit currents. Despite the reduced output voltage, the results clearly show an elevated component of field current at the pole-passing frequency of 120 Hz. This result concurs with FEA simulation results.

To increase overall brush resistance, the brushes were intentionally compromised as shown in Fig. 17. With these worn brushes, the machine was again run in generator mode under the same conditions. Very little change in the armature or field currents was evident when compared with the baseline; however, the transfer impedance dropped from the baseline value of 217.3 to 208. This effect was also predicted by the coupled FEA simulations.
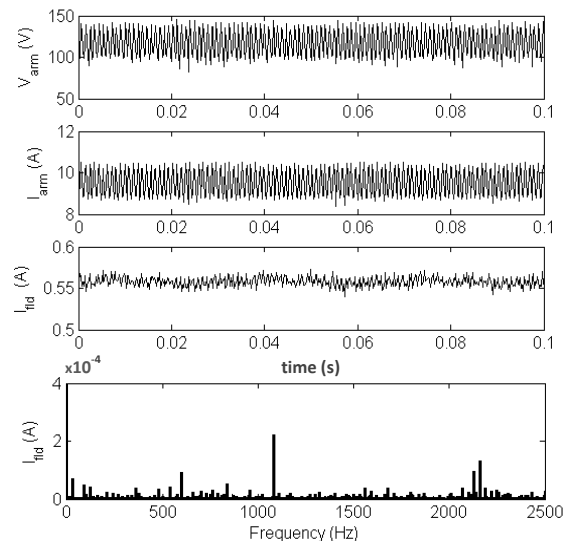

Figure 13: Experimental DC machine

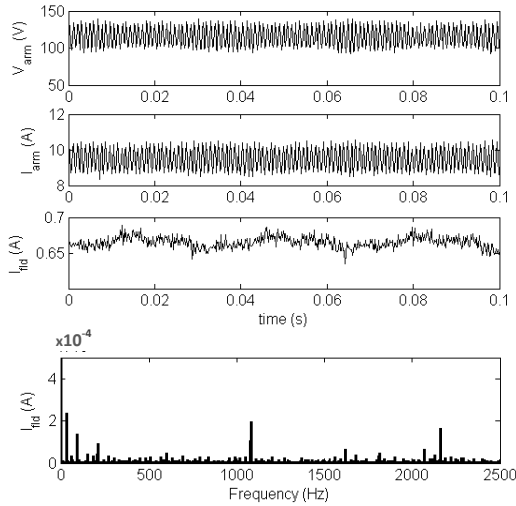Figure 14: Experimental baseline results
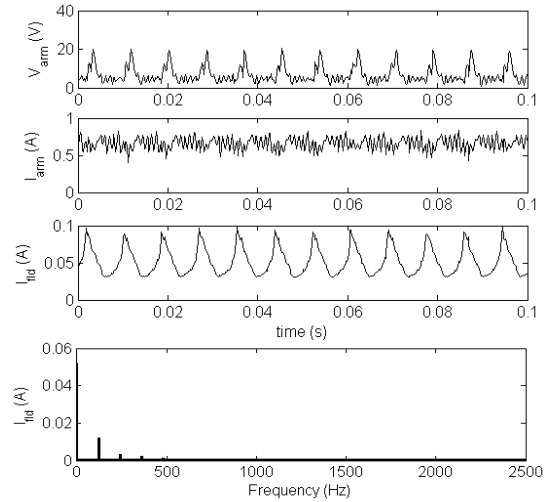
Figure 15: Field winding fault experiment

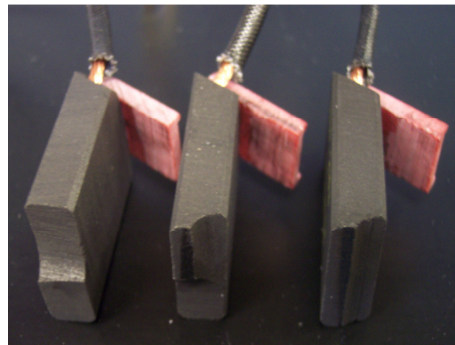Figure 16: Armature short experiment

Figure 17: Compromised brushes

Conclusions

A method for detailed analysis of the brushed DC machine operating under fault conditions is presented. The proposed method has been used to analyze the brushed DC machine under conditions including armature short circuit and open circuit, short-circuit field winding, bad commutator segment, and brush degradation. From these simulations, several important parameters were identified that may indicate the onset of DC machine faults. Those parameters are the transfer impedance and the field current component at both the pole-passing and commutation frequency. Laboratory seeded fault tests on a DC machine were then used to confirm the effect of various faults on the identified observables. The results of this study can be used as a starting point for a predictive diagnostics implementation for DC machinery.

The views and conclusions contained in this document are those of the authors and should not be interpreted as representing the official policies, either expressed or implied of the Aviation Applied Technology Directorate or the United States Government.

References

[1] Z. Glowacz, and A. Zdrojewski, "Mathematical Modeling of Commutator DC Motor in Failure Conditions," in *5th IEEE International Symposium on Diagnostics for Electric Machines, Power Electronics, and Drives (SDEMPED)*, 2005, pp. 1-5.

[2] Z. Glowacz, and A. Zdrojewski, "Diagnostics of Commutator DC Motor Basing on Spectral Analysis of Signals," in *IEEE International Symposium on Diagnostics for Electric Machines, Power Electronics, and Drives (SDEMPED)*, 2007, pp. 497-500.

[3] R. Retana, A. Paweletz, and H. Herzog, "Analysis and Detection of Short Circuits in Fractional Horsepower Commutator Machines," *IEEE Transactions on Energy Conversion*, vol. 23, no. 2, pp. 484-491, June 2008.

[4] M. Liu, X. Yang, and S. Cui, "Online Fault Detection and Diagnosis of Permanent-magnetic DC Motor," in *IEEE Vehicle Power and Propulsion Conference*, 2008, pp. 1-5.

[5] G. Kliman, and D. Song, "Remote Monitoring of DC Motor Sparking by Wavelet Analysis of the Current," in *IEEE International Symposium on Diagnostics for Electric Machines, Power Electronics, and Drives (SDEMPED)*, 2003, pp. 25-27.

[6] S. Barwany, and G. Thomas, "A Non-intrusive System (SMS) to Monitor Sparking Along the Brush/Commutator Interface of a DC Machine," in *5th International Conference on Electrical Machines and Drives*, 1991, pp. 72-76.

[7] R. Wang, and R. Walter, "Modeling of Universal Motor Performance and Brush Commutation Using Finite Element Computed Inductance and Resistance Matrices," *IEEE Transactions on Energy Conversion*, vol. 15, no. 3, pp. 257-263, 2000.

[8] D. C. Meeker, Finite Element Method Magnetics, Version 4.0.1 (03Dec2006 Build), http://www.femm.info

[9] K. Sawa, H. Yamamoto, and K. Miyachi, "Analysis of Armature Circuit Inductance of DC Machines by FEM," *IEE Proceedings on Electric Power Applications*, vol. 132, no. 6, 1985, pp. 307-314.

Biography

TODD D. BATZEL received a BS in electrical engineering from Pennsylvania State University in 1984, an MS in electrical engineering from the University of Pittsburgh in 1989, and a PhD in electrical engineering in 2000 from Pennsylvania State University. He is currently an associate professor of electrical engineering at Penn State Altoona. His research interests include machine controls, electric drives, and artificial intelligence.

NICHOLAS C. BECKER is currently a fourth-year student in the electro-mechanical engineering technology program at Penn State Altoona. His research interests include electrical machinery systems and applications.

MIHAI COMANESCU received his BSEE from Bucharest Polytechnic University in 1992 and his MS and PhD from Ohio State University in 2001 and 2005, respectively. He is

currently an assistant professor of electrical engineering at Penn State Altoona. His research interests are power electronics, AC drives, and motion control systems.